



**HAL**  
open science

## Surface topography in ball end milling process: Description of a 3D surface roughness parameter

Yann Quinsat, Laurent Sabourin, Claire Lartigue

### ► To cite this version:

Yann Quinsat, Laurent Sabourin, Claire Lartigue. Surface topography in ball end milling process: Description of a 3D surface roughness parameter. *Journal of Materials Processing Technology*, 2007, pp.135-143. hal-01154042

**HAL Id: hal-01154042**

**<https://hal.science/hal-01154042>**

Submitted on 21 May 2015

**HAL** is a multi-disciplinary open access archive for the deposit and dissemination of scientific research documents, whether they are published or not. The documents may come from teaching and research institutions in France or abroad, or from public or private research centers.

L'archive ouverte pluridisciplinaire **HAL**, est destinée au dépôt et à la diffusion de documents scientifiques de niveau recherche, publiés ou non, émanant des établissements d'enseignement et de recherche français ou étrangers, des laboratoires publics ou privés.

# Surface topography in ball end milling process: description of a 3D surface roughness parameter

Y. Quinsat<sup>(a)\*</sup>, L. Sabourin<sup>(b)</sup>, C. Lartigue<sup>(c)</sup>

(a) LURPA/ENS de Cachan 61 avenue du Président Wilson 94235 Cachan Cedex France, (b) LaMI/ IFMA campus des cézeaux 63165 Aubière cedex France, (c) LURPA/IUT de Cachan université Paris sud 11, 9 avenue division Leclerc 94234 Cachan Cedex France.

\* Corresponding author Phone: 331 47 40 22 15, Fax : 3301 47 40 22 20, email: quinsat@lurpa.ens-cachan.fr

## ABSTRACT

In the field of free-form machining, CAM software offers various modes of tool-path generation, depending on the geometry of the surface to be machined. Manufactured surface quality results from the choice of machining strategy and machining parameters. The objective of this paper is to provide a 3D surface roughness parameter that formalizes the relative influence of both machining parameters and surface requirements. This roughness parameter is deduced from simulations of the 3D surface topography obtained after three-axis machining using a ball-end cutter tool. Following a state-of-the-art assessment of surface roughness characterization, this paper will present the model generating these simulations before proceeding with an experimental verification campaign of the pattern left on the machined surface. An analysis of the patterns obtained for various sets of machining parameters serves to highlight those that influence 3D surface topography. The 3D surface roughness parameter is therefore defined according to both an influential machining strategy parameter and the surface description. An illustration will be proposed in the article's final section of an industrial case for which the 3D parameter has been used to determine the machining parameters that lead to the expected level of surface roughness.

## KEYWORDS

Machining strategy, Surface roughness, Ball end milling, 3D Surface topography

## 1. Introduction

The machining of free-form surfaces along three axes using a ball-end cutter tool is generally performed in accordance with a given machining strategy. Such a strategy for the finishing process must incorporate a geometric feature into its final form [1]. From a geometric point of view, the main parameters defining a machining strategy are [2]:

- machining direction (or sweeping direction),
- transverse step, and
- longitudinal step.

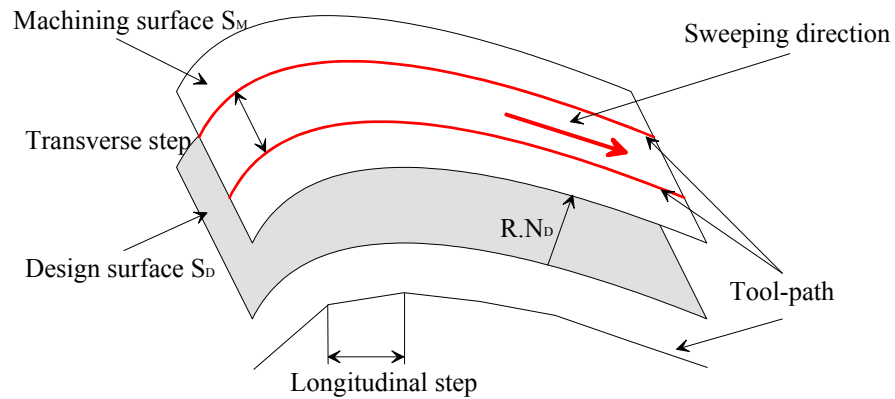


Fig. 1: Machining strategy parameters

Within a competitive economic context, it is necessary to reduce costs and meet functional requirements. Choosing a machining strategy thus proves to be an optimization problem submitted to constraints based on the geometry of the surface to be machined. Machining time actually depends on both the part geometry and efficiency of the calculated tool path; the same applies for the geometric surface quality, which results from the tool movement calculated based on the machining strategy. The optimization problem has been more generally studied in the literature, with the objective of reducing either cutting time [3] or unproductive time [4,5]. Only a few previous efforts have examined studies in the aim of identifying machining strategy parameters that optimize surface quality requirements [6,7,8]. One difficulty encountered is the lack of a 3D criterion for evaluating geometric surface quality; this may be related to both the geometric specifications and machining strategy. The manufactured surface quality stems from the correlation between the computed tool path and the primary cutting motion. The tool path is computed as a set of characteristic points transmitted to the numerical controller (NC unit); linear interpolation would commonly be employed herein. In the machining direction therefore, cutter location (CL) points are calculated along the longitudinal step characterizing the distance between two successive points. The machining tolerance (see Fig. 2) allows calculating the longitudinal step with respect to the tool path radius of curvature [9]: the higher the radius of curvature, the larger the longitudinal step.

Moreover, since surface machining is obtained by means of tool sweeping, a cusp remains from the trace left by the tool on the surface. From a more general standpoint, the transverse step is calculated from the maximum allowed scallop height. The global transverse step  $p_1$  is defined in a plane normal to the tool axis  $\mathbf{k}$ , while the local transverse step  $p$  is defined in the  $(\mathbf{n}', \mathbf{d}_T)$  plane (Fig. 2).

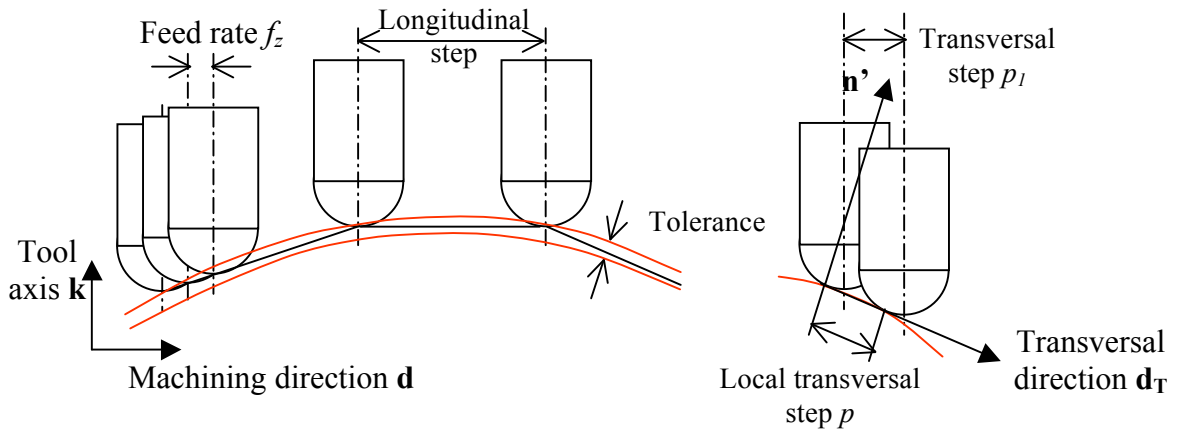


Fig. 2: Parameter description

In considering the cutting motion, both the feed rate and tool rotation serve to define a periodic phenomenon that gets combined with the tool path in order to generate the machined surface. Should the longitudinal step be greater than the feed rate ( $f_z$ ), the tool path computation error would be of a higher order than surface roughness (Fig. 3) [2].

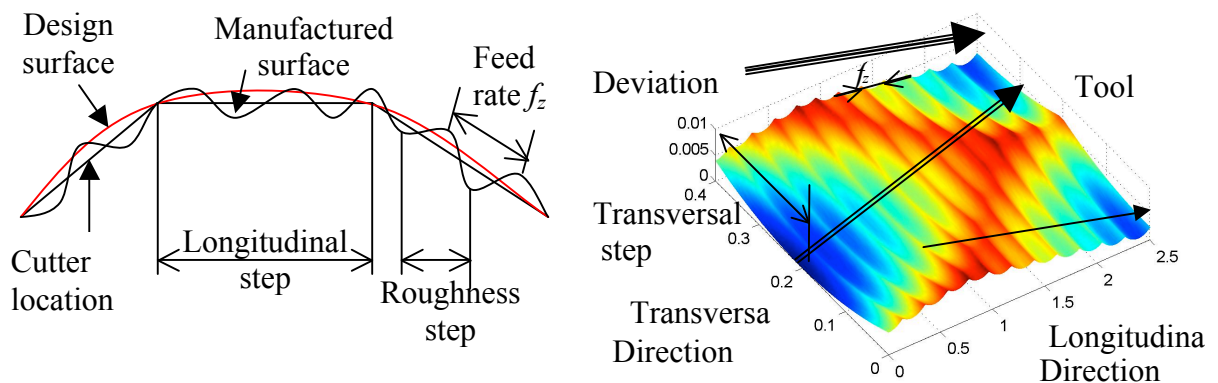


Fig. 3: Surface roughness linked to tool-path generation

The machining tolerance  $t$  and transverse step  $p_1$  exert significant influence on the pattern left on the machined part. In an initial approach, the longitudinal step is presumed to be greater

than the feed rate, i.e.: tolerance  $t$  is assumed of a higher order than surface roughness.

Furthermore, machining tolerance is considered to be less than the transverse step in order to neglect the orange skin effect. These two assumptions are incompatible given that a small machining tolerance reduces the longitudinal step. These conditions are only met on smooth surfaces with high transverse and longitudinal radius of curvature values. It is still necessary however to tie these parameters on the basis of intended machined surface function.

The objective of the proposed work program therefore is to define a 3D surface roughness parameter that:

- provides a formal description of the relative influence of each machining strategy parameter on the surface quality (i.e. machining direction, transverse step, longitudinal step, feed rate);
- proves capable of describing the surface requirements.

This criterion will allow choosing the optimal machining strategy to attain for a given surface quality.

The paper has been organized as follows. The first section introduces the tool path computation parameters. Section 2 will then present the state-of-the-art on characterizing surface roughness. Section 3 is devoted to our proposed model and followed by simulation and validation exercises. The model has been built by considering that during the milling operation, the cutting edges undergo a combined motion of translation and rotation.

Simulations serve to define a surface roughness parameter correlated with the machining strategy. Validations are carried out subsequent to the three-axis milling of plane surfaces under various cutting conditions via the experimental measurements of surface roughness.

The 3D roughness parameter gets used in an application to an industrial case in the paper's final section.

## **2. 3D surface roughness**

Sculpted part surfaces are most generally defined from parameterized surfaces, for which the characteristic differential properties depend on the particular point. From a functional perspective, standardized specifications come in four types: dimensional, shape defect (ISO 1101), surface roughness (ISO 1302), and visual aspect (ISO 8785). This paper will focus on the surface roughness requirement.

### **2.1 Characteristic parameters**

Surface roughness is classically described through 2D parameters such as ( $R_a$ ,  $R_t$ ,  $R_z$ ), defined from a 2D profile [ISO 1302]. This approach has two major disadvantages. The first pertains to the representation of functional requirements. Profiles can indeed display identical roughness parameters, yet contain different mechanical properties. The second disadvantage pertains to measurement direction: parameters are confined to a single direction and do not represent the roughness of the entire surface [10,11]. Depending on the plane in which the profile is measured, results may differ. A coupling of the effects from feed rate  $f_z$  and transverse step  $p$  however leads to an actual 3D surface finish, while a unidirectional measurement cannot yield an accurate image of this coupling.

With advances in 3D measurement systems, in particular by means of optical techniques, it is now possible to measure the 3D surface finish with good precision [12,13]. Defining new parameters to depict 3D surface roughness has thus become necessary. A standardization project underway (BRC 3374/1/0/170/90/2) proposes establishing such a set of parameters. These parameters are calculated from the mathematical representation of a surface  $\eta(x,y)$  and are simply extensions to the 3D case of 2D parameters [14]. Even though these latest

parameters are defined similarly to those laid out in the standard [ISO 12085], they are not really correlated with functional requirements.

Arithmetic deviation	$S_a = (1/(l_x \cdot l_y)) \iint_S  \eta(x,y)  \cdot dx \cdot dy$
Root mean square deviation	$S_q = \sqrt{(1/(l_x \cdot l_y)) \iint_S (\eta(x,y))^2 \cdot dx \cdot dy}$
Highest peak of the surface	$S_p = \max(\eta(x,y))$
Lowest valley of the surface	$S_v = \min(\eta(x,y))$
Height deviation	$S_z = ( S_p  +  S_v )$

Tab 1: Parameters for 3D surface roughness

Recent work has focused on characterizing surface geometry using fractal dimensions [15,16], which provide a good indicator of the surface complexity: the fractal dimension increases as surface roughness increases. Other authors have proposed models for describing homogeneous topography, with such models being introduced for the purpose of describing surface roughness using just one parameter [17,18].

The use of 3D indicators to represent 3D surface topography would therefore seem to be effective. A description of the 3D pattern obtained after surface machining is nevertheless essential both to highlight the influence of machining parameters on surface roughness and to link surface roughness with functional requirements.

## 2.2 Characterization of 3D surface topography in 3 axis machining

As of now, few formalized studies have been conducted on the surface roughness prediction for ball-end milled surfaces [19]. Some previous work has focused on the influence of machining strategy parameters. Two frames of reference can be adopted:

- The experimental standpoint: the modeling of 3D topography results from an analysis of measured surfaces, and
- The theoretical standpoint: the 3D topography is derived by simulating the tool movement envelope during machining.

### **2.2.1 Experimental standpoint**

As for the experimental standpoint, the majority of results are qualitative and seek to correlate the surface quality obtained with machining parameters. For instance, Ramos presented a series of observations on how machining direction influences surface quality following the machining of a boat propeller [20]. M.C. Kang showed the various topographies obtained on surfaces machined using different tool orientations [6]. The author analyzed 2D pictures of the patterns and recommended avoiding all upward and downward milling. Machining in the slope direction does generate a greater number of imprints on the part.

R. Baptista developed a model that correlated feed rate, transverse step and surface roughness  $Ra=F(f_z,p)$  [21]. The model built from experimental work is only adapted to the ball-end cutter machining of an aluminum part. Other work performed has extended the model by adding the influence from part geometry, including surface orientation [7,22,23]. The results obtained reveal a variation in surface quality as a function of both feed rate and orientation. These variations however remain insignificant in comparison with measurement errors [24]. In addition, the results obtained exhibit too much variability to be useful [7].

All of the research referenced above has been based on experimental studies. Their respective fields of validity are thus highly correlated with experimental conditions (materials, tools, ranges). Not one of these studies however actually allows tying machining strategy parameters to surface roughness.

### **2.2.2 Theoretical standpoint**

Beyond these experimental models, a number of theoretical models have also been proposed. B.H. Kim described the texture found in ball-end milling using numerical simulations [25]. This effort sought to refine the standard model that correlates scallop height with transverse



step. The influence of feed rate has been taken into account, yet tool orientation has not. More recently, K.D. Bouzakis incorporated the influence of tool orientation and focused on the cutting edge motion. The simulations calculated showed the influence of tool orientation, transverse step and feed rate on surface quality [26]. C.K. Toh has complemented this work by defining the best direction for machining an inclined plane [27].

None of these references however allow linking machining parameters to a 3D surface quality criterion. As a case in point, defects (i.e. machining tolerance) due to the tool path computation are not taken into account.

In order to define a 3D surface quality parameter relative to the machining process, the influence on surface roughness from the tool orientation with respect to the surface, the transverse step, the feed rate, and longitudinal step must be identify and then characterize.

The transverse step and feed rate parameters exert influence in both the longitudinal and transverse directions. This finding required us to introduce a surface criterion. As an initial procedure, the longitudinal step does not enter into the surface roughness computation. Since the calculated topography is related to the machining of a plane surface, the longitudinal step is theoretically equal to the length of the tool path.

### **3. 3D Surface topography in 3 axis machining**

The proposed approach is more heavily dedicated to evaluating the pattern obtained on the machined surface rather than the actual surface roughness. For the sake of simplicity, this approach will first be developed using a plane surface. The machined surface can in fact be locally approximated by its tangent plane at the considered point.

$\alpha_L$  $\alpha_T$  $\alpha_T$  $\mathbf{k}_o$  $\psi$  $\mathbf{j}_o$  $\theta$ 

In this section, cutting edge motion vs. tool orientation will be examined. It has been assumed

herein that the cutting edge is a perfectly-circular curve and that only points at the lowest

altitude leave a lasting imprint on the part.

Fig. 4: Possible orientations of the tool axis for a given feed direction

Fig. 5: Description of the parameters

### 3.1 Calculation of the pattern obtained by the ball end cutter tool

Let  $\mathfrak{R}_{Part} = (O_{Pr}, \mathbf{i}_p, \mathbf{j}_p, \mathbf{k}_p)$  be the reference frame related to the part where:

- $\mathbf{k}_p$  is the normal to the plane to be machined.
- $\mathbf{i}_p$  defines the direction of the straight lines parallel to the tool-paths.
- $\mathbf{j}_p$  is given by the cross product  $\mathbf{j}_p = \mathbf{k}_p \otimes \mathbf{i}_p$

Now, let  $\mathfrak{R}_{tool} = (O, \mathbf{i}_o, \mathbf{j}_o, \mathbf{k}_o)$  be the frame linked to the tool, where:

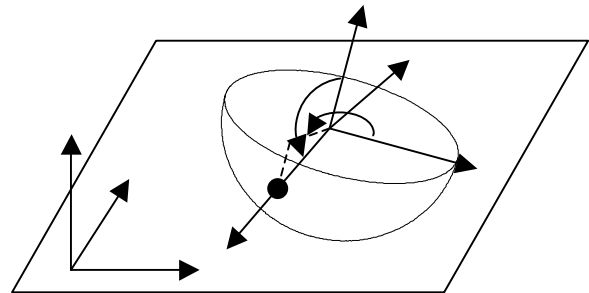
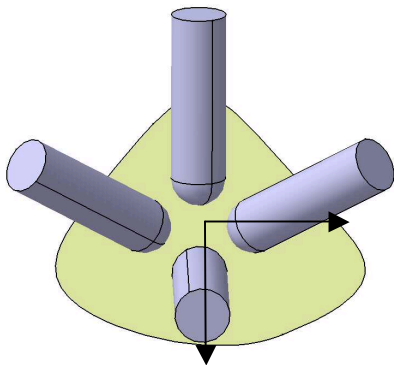
- O is the centre of the half sphere the radius of which is R.
- $\mathbf{k}_o$  defines the tool axis direction.

The directing vectors are given by the following relationship:

$$\begin{pmatrix} i_o \\ j_o \\ k_o \end{pmatrix} = \mathbf{R}_{op} \cdot \begin{pmatrix} i_p \\ j_p \\ k_p \end{pmatrix} \quad (1)$$

Where  $\mathbf{R}_{op}$  is the matrix denoting frame changes that, for a longitudinal inclination, can be expressed by (see Fig. 4):

$$\mathbf{R}_{op} = \begin{pmatrix} \cos(\alpha_L) & 0 & -\sin(\alpha_L) \\ 0 & 0 & 0 \\ \sin(\alpha_L) & 0 & \cos(\alpha_L) \end{pmatrix} \quad (2)$$



In order to parameterize the curve that defines the cutting edge, a spherical frame is associated to the half-sphere, whereby:  $\mathfrak{R}_{\text{spherical}}=(O, \mathbf{u}_r, \mathbf{u}_\theta, \mathbf{u}_\psi)$  with  $\psi$  the angle between  $\mathbf{u}_r$  and  $\mathbf{k}_o$ , and  $\theta$  the rotational angle measured in the  $(\mathbf{i}_o, \mathbf{j}_o)$  plane (Fig. 5). The cutting edge is then defined as the curve  $C(\psi)$ .

For the  $i^{\text{th}}$  tool path, let  $\mathbf{O}_p \mathbf{O} = \mathbf{T}_i(t)$  be the tool trajectory with respect to the tool displacement direction. The tool rotation is given by:  $\mathbf{\Omega} = \mathbf{\Omega} \cdot \mathbf{k}_o$ .

To compute the imprint left by the tool, the cutting edge position must be defined within the part frame. The position of a point  $M$  belonging to the cutting edge is given by:  $\mathbf{OM} = C(\psi) \cdot \mathbf{u}_r$ .

This expression then leads to:

$$\begin{pmatrix} (x - T_{ix}(t)) \\ (y - T_{iy}(t)) \\ (z - T_{iz}(t)) \end{pmatrix} = R_{op}^{-1} \cdot C(\psi) \cdot \begin{pmatrix} \sin \psi \cdot \cos \theta \\ \sin \psi \cdot \sin \theta \\ \cos \psi \end{pmatrix} \quad (3)$$

The following step consists of calculating the intersection between the curve and the set of planes associated with the displacement. This step is carried out by solving for various values of  $(x, t)$  from the previous non-linear system (see Equation 3), for which the unknowns are  $(y, z, \psi)$ . The angle  $\theta$  is given by:  $\theta = \mathbf{\Omega} \cdot t + \theta_0$ . For each  $t$ , a set of triplets  $E=(x, y, z)$  that define intersecting points is obtained (Fig. 6). The final imprint left by the tool corresponds to a solution that, for the same given location in the tangent plane  $(x, y)$ , displays the lowest altitude.

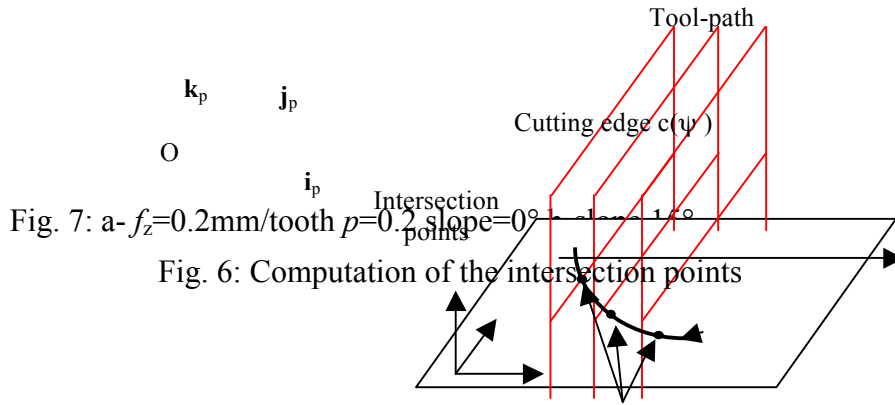
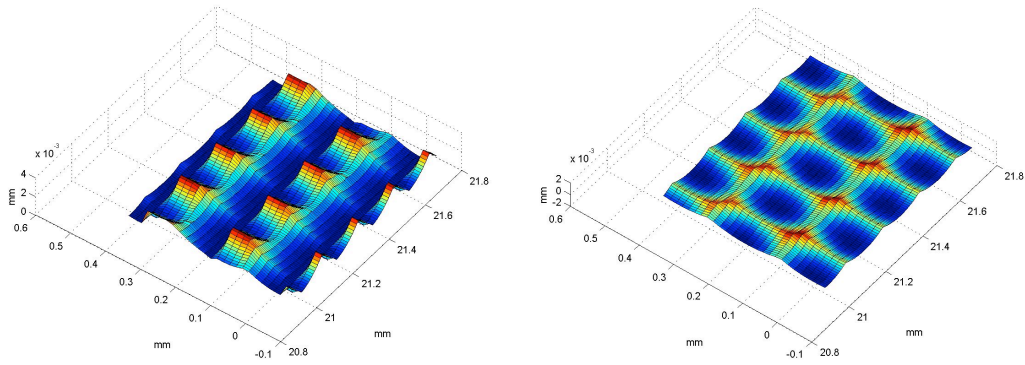


Fig. 7: a-  $f_z=0.2\text{mm/tooth}$   $p=0.2$  slope= $0^\circ$



Various patterns are calculated for different sets of parameters. Only longitudinal (Fig. 4  $\alpha_L$ - $\alpha_L^+$ ) or transverse (Fig. 4  $\alpha_T$ - $\alpha_T^+$ ) slopes has been considered. The results presented in Figure 7 demonstrate the influence of both feed rate ( $f_z$ ) and transverse step ( $p$ ). It should be remarked that the amplitude of surface defects ( $S_z$ ) decreases from  $15\mu\text{m}$  to  $6\mu\text{m}$  with the slope of the tool (either longitudinal or transverse slope). In contrast, for an inclined angle greater than *the limit angle*  $\alpha=g(f_z,p,R)$  (Fig. 8), neither the magnitude nor the shape of the imprint left by the tool undergo any influence ( $\text{magnitude}\approx 6\mu\text{m}$ ). The limit angle is calculated by:  $\cos(\alpha)=L/R$ , where  $L=f_z$  or  $L=R$  depending on whether the slope is longitudinal or transverse.

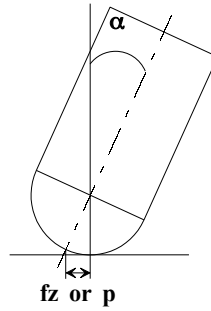


Fig. 8: Calculation of the limit angle

When a slope steeper than the limit angle  $\alpha$  has been chosen, the pattern is a compound of spherical segments, with the radius of each segment equaling the tool radius  $R$ . The pattern therefore solely depends on feed rate ( $f_z$ ), transverse step ( $p$ ) and tool radius ( $R$ ). The tool/surface contact position exerts no influence.

### 3.2. Experiments

In order to compare the theoretical results with actual surface roughness, a series of sweepings over planes were carried out with various orientations relative to the tool axis (from  $0^\circ$  to  $30^\circ$  with a  $5^\circ$  increment) (see Fig. 9). For each case, the tool follows a square path, thereby making it possible to study the influence of both the longitudinal and transverse slopes. Tests are carried out on a high-speed milling machine tool with experimental conditions as given in Table 2.

Tool diameter	10 mm
Spindle rotation	18000 rpm
Feed rate	0.2 mm/tooth et 0.3 mm/tooth
Material	AU4G

Table 2

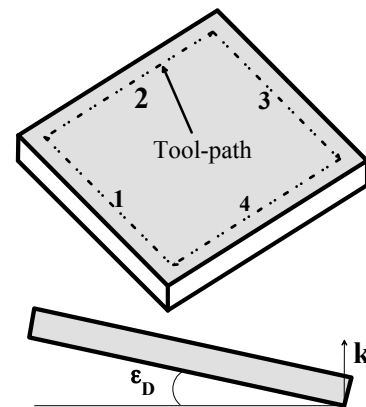


Fig. 9: Description of the tool-paths used

The surfaces obtained are measured using an optical instrument (Wyko NT1100 - <http://www.veeco.com/>) (see Fig. 10). When the slope is  $0^\circ$ , surface quality is very poor and does not allow for accurate measurements. For a slope steeper than  $5^\circ$ , both the patterns and defect amplitudes are similar to those calculated from the simulations (see Figs. 7 and 10 for a

slope of 15°). Simulations are thus in good agreement with experimental findings, which leads to validating the model proposed to predict surface topography. This model reveals that when surfaces are oriented within a range between 0° and 30°, the machining direction does not exert any influence on the surface pattern obtained. Hence the primary parameters influencing surface quality are feed rate ( $f_z$ ) and transverse step ( $p$ ). Although the pattern is similar to that obtained by Kang [6] and more recently by Toh [27], the machining direction (either upward or downward) was not found to be of any influence (Fig. 10).

### 3.3 3D surface roughness parameter

Simulations and tests have shown that for small slopes, the pattern consists of a compound of spherical segments. At present, no standardized parameter is available for describing such a pattern. Moreover, the classical parameters ( $R_a$ ,  $R_t$ ) do not highlight any coupling between feed rate and transverse step. To define the surface roughness that corresponds to this type of pattern, the surface parameter  $S_z$  can be employed:  $S_z=(|\max(\eta(x,y))|+|\min(\eta(x,y))|)$  (see Table 1). This parameter corresponds to the height deviation between lowest and highest points on the surface. For a spherical segment of radius  $R_o$ , limited by  $f_z$  and  $p$ , the maximum height lies at one of the vertices of the rectangle defined by  $f_z$  and  $p$ , and  $S_z$  can thus be expressed by:

$$S_z = R_o - (R_o^2 - \frac{f_z^2 + p^2}{4})^{1/2} \quad (4)$$

During the finishing process, the feed rate  $f_z$  and transverse step  $p$  equal approximately 0.2 mm. Generally speaking, the radius of the tool used exceeds 4 mm. Consequently, the term  $f_z^2 + p^2$  is very small in comparison with  $R_o^2$ , which leads to simplifying the previous expression into:

$$S_z = \frac{f_z^2 + p^2}{8.R_o} \quad (5)$$

The 3D parameters  $S_z$  defined in Equation 5 are thus representative of surface quality and correlated with the influential machining parameters. The objective now is to define a similar

3D parameter for a 3D free-form surface that links 3D surface roughness  $S_z$  to the machining strategy parameters.

#### 4 Study of a 3D free-form surface

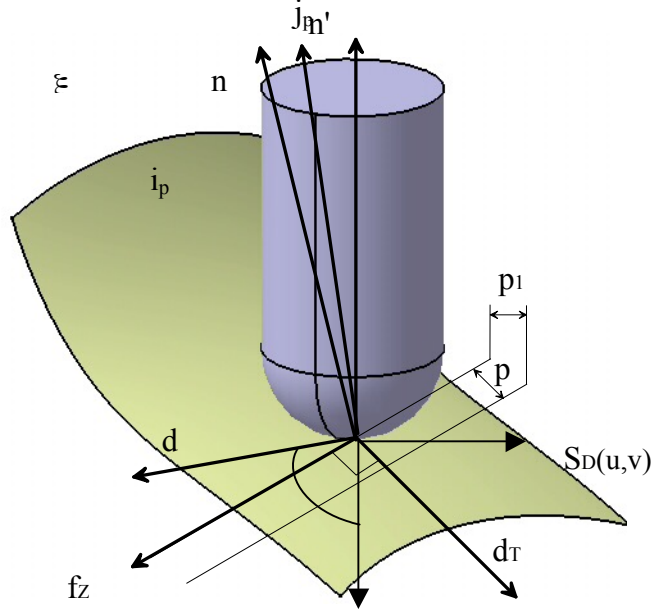


Fig. 11: Parameter description.

The surface is defined by its parametric form  $S_D(u,v)$ , assumed to be differential to the first order (see Fig. 11). The normal can thus be calculated by:

$$n(u,v) = \frac{\frac{\partial S(u,v)}{\partial u} \times \frac{\partial S(u,v)}{\partial v}}{\left\| \frac{\partial S(u,v)}{\partial u} \times \frac{\partial S(u,v)}{\partial v} \right\|} \quad (6)$$

For a given point on the surface, the machining direction is denoted  $d$ , where  $d = \begin{pmatrix} \cos \xi \\ \sin \xi \\ 0 \end{pmatrix}$ , with

$\xi$  defining the orientation of  $d$  with respect to the  $x$  axis in the  $(i_p, j_p)$  plane. Locally, the tool path is assumed to belong to the tangent plane of the surface at that given point.

The transverse direction  $d_T$  thus verifies:

$$\begin{cases} d_T \cdot n = 0 \\ d_T \cdot d = 0 \end{cases} \quad (7)$$

Hence  $d_T$  is perpendicular to the  $P_n = (d, n)$  plane, and the following definition is choose:

$$d_T = (d \otimes n) / (\|d \otimes n\|) \quad (8)$$

Next, vector  $n'$  is given by  $n' = d_T \times d$ , which leads to two cases:

- either  $\mathbf{n}'$  is outward oriented:  $\mathbf{n}'$  and  $\mathbf{k}_p$  form an acute angle (the surface contains no undercut), and  $\mathbf{n}' \cdot \mathbf{k}_p = \cos\beta$ ;
- or  $\mathbf{n}'$  is outward oriented:  $\mathbf{n}'$  and  $\mathbf{k}_p$  form an obtuse angle, and  $\mathbf{n}' \cdot \mathbf{k}_p = \cos(\pi-\beta) = -\cos\beta$ .

Generically speaking, the expression of  $\beta$  is:  $\beta = \arccos(|\mathbf{n}' \cdot \mathbf{k}_p|)$ .

The effective height of pattern  $S_z$  was defined in the previous section by means of Equation (5). Since the surface is locally approximated by a plane at the target point  $M$  and considering that  $p = p_1 / \cos\beta$  with  $p_1$  the transverse step chosen for the whole part,  $S_z$  can be expressed by:

$$S_z = \frac{p_1^2 / \cos^2 \beta + f_z^2}{8.R_o} \quad (9)$$

$\beta$  depends upon both the selected machining direction and the normal to the surface at the point  $M$ . By replacing  $\beta$  in this equation, the surface roughness calculation becomes:

$$S_z = \frac{p_1^2 / \left( \left( \frac{\mathbf{d} \otimes \mathbf{n}}{\|\mathbf{d} \otimes \mathbf{n}\|} \otimes \mathbf{d} \right) \cdot \mathbf{k}_p \right)^2 + f_z^2}{8.R_o} \quad (10)$$

The previous equation correlates both the local surface normal ( $\mathbf{n}$ ) and machining strategy ( $\mathbf{d}$ ,  $p_1, f_z$ ) with surface quality. The next section will discuss how the surface roughness parameter can be used to define machining parameters for an industrial case.

### 5 Application : An industrial case study

In this section, the machining of a surface corresponding to a die used in the automotive industry will be studied. Our objective here is to measure surface roughness across various representative regions and then to correlate these results with our model output. The selected cutting conditions correspond to those applied in industry for the machining of aluminum alloy 7075 (Fortal HR, Pechiney). This material enhances the visual aspect of the surface. To



Region (a)

Region (b)

Region (c)

Small radius guarantee a surface roughness  $S_z=5 \mu\text{m}$ , the largest transverse step is determining, for a given machining direction, by implementation of Equation (10).

Programmed feed rate $V_f$	$6 \text{ m} \cdot \text{min}^{-1}$
Spindle rotation N	15000 rpm
Feed /tooth $f_z$	0.2 mm/tooth
Tool radius $R_o$	5 mm
Tooth number	2
Cutting speed $V_c$	$470 \text{ m} \cdot \text{min}^{-1}$

Table 3: Cutting conditions

The machined surface is measured in three regions using an optical measurement Wyko NT1100 (Fig. 12) corresponding to:

- a tight region (a),
- a convex region (b), and
- a concave region (c).

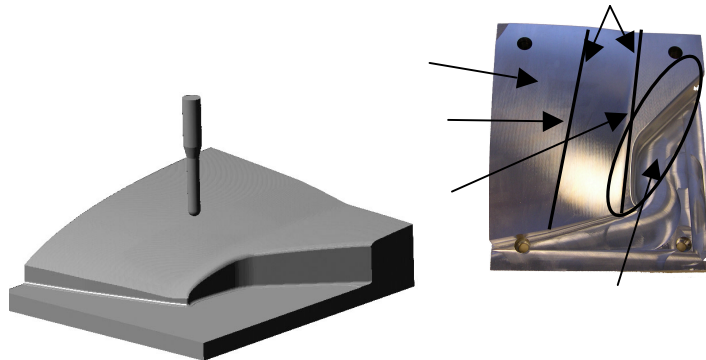


Fig. 12: Description of the measured regions

The results presented in Figure 13 show that the pattern obtained on the part is actually a set of spherical segments. Surface roughness measurements (Table 4 below) indicate that the value of  $S_z=5 \mu\text{m}$  has not been respected, as the recorded values are all oscillating around  $10 \mu\text{m}$ .

$S_z (\mu\text{m})$	
Region (a)	9,1
Region (b)	12,4
Region (c)	8,45

Table 4 : Measured surface roughness

Moreover, the dimension of sphere caps in the longitudinal direction is 0.4 mm and not the programmed 0.2 mm: the feed rate is actually twice the programmed rate. This variation serves to increase surface roughness. For the same transverse step, yet a feed rate value equal to 0.4 mm, the theoretical  $S_z$  calculated using Equation (10) then amounts to 8  $\mu\text{m}$ . This variation can be explained by the influence of tool eccentricity. A low tool eccentricity value is indeed sufficient to introduce one of the two cutting edges into the pattern computation. The feed rate for the surface roughness  $S_z$  calculation thus gets doubled. By taking into account the actual size of the spherical segment, the theoretical surface roughness (8  $\mu\text{m}$ ) is close to the measured surface roughness for regions (a) and (c). In the case of region (b), the variation between theoretical and measured surface roughness values is greater. In order to calculate  $S_z$ , the surface is locally approximated by a plane: this assumption is clearly not valid in region (b), over which the curvature is small, and corresponds to our model limit.

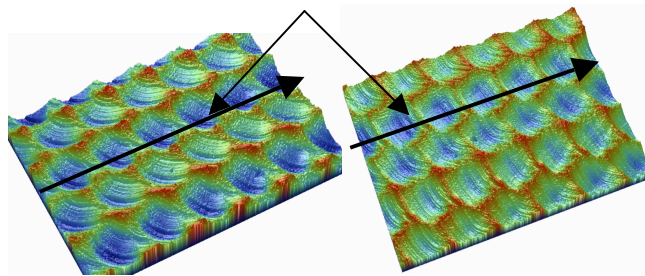


Fig. 13: Measured pattern on the die surface

## 6. Conclusion

This paper has focused on free-form surface machining. The objective here is to produce a 3D surface roughness parameter that formalizes the influence of machining parameters and that can be correlated with surface requirements. Recent needs in the area of surface roughness characterization have underscored the pertinence of using a 3D parameter. To define this 3D parameter, a simulation model of the 3D topography has been proposed for three-axis

machining using a ball-end cutter tool. The model was established in considering that during milling, the cutting edges are in a combined translation and rotation motion. The model was first developed for machining a plane surface that allows comparing simulations to experimental test results. This comparison showed the efficiency of our model; we were able to determine the influential machining parameter by use of various sets of parameters that lead to defining a 3D surface roughness parameter with respect to both machining strategy and surface description. The extension of this parameter to free-form surfaces has also been detailed. The application to an industrial case has highlighted the limitations of this model, which is based on an ideal tool geometry.

This paper however has shown that a description of the 3D pattern obtained after surface machining is essential in order to expose the influence of machining parameters on surface roughness and to correlate surface roughness with functional requirements. An initial step has been accomplished by linking surface topography to machining parameters. To improve the effectiveness of our model, actual tool geometry must be taken into account. Subsequent work will also focus on the connection between the 3D pattern and surface requirements.

## References

- [1] Y. Quinsat, L. Sabourin, Optimal selection of machining direction for 3 axis milling of sculptured parts, *International Journal of Advanced Manufacturing Technology*, online 30 march 2005.
- [2] C. Lartigue, E. Duc, C. Tournier, Machining of Free-Form Surfaces and Geometrical Specifications, *Proc Instn Mech Engrs* 213 (1999) 21-27.
- [3] M. Held, E. M. Arkin, C. L. Smith, Optimization problems related to zigzag pocket machining, *Algorithmica* 26 (2001) 219-236.
- [4] Z. Chen, Z. Dong, G. W. Vickers, Automated Surface Subdivision and Tool Path Generation for 3 1/2 1/2 axis CNC Machining of Sculptured parts, *Computer in Industry*, 50 (2003) 319-331.
- [5] C- J. Chiou, Y. S. Lee, A Machining potential field approach to tool path generation for multi-axis sculptured surface machining, *Computer Aided Design*, 34 (2002) 357-371.
- [6] M. C. Kang, K. K. Kim, D. W. Lee, J. S. Kim, N. K. Kim, Characteristics of inclined Planes According to the Variations of the cutting direction in high-speed ball-end milling, *International Journal of Advanced Manufacturing Technology* 17 (2001) 323-329.

- [7] T. J. Ko, H. S. Kim, S. S. Lee, Selection of the machining inclination angle in high-speed ball end milling, *International Journal of Advanced Manufacturing Technology* 17 (2001) 163-170.
- [8] C. M. Lee, S. W. Kim, K. H. Choi, D. W. Lee, Evaluation of cutter orientations in high-speed ball end milling of cantilever-shaped thin plate *Journal of Material Processing Technology* 140 (2003) 231-236.
- [9] K. Choi, R. B. Jerard, *Sculptured surface machining theory and application*. Kluwer Academic Publisher 1998.
- [10] W. P. Dong, P. J. Sullivan, K. J. Stout, Comprehensive study of parameters for characterizing three dimensional surface topography I: Some inherent properties of parameter variation *Wear* 159 (1992) 161-171.
- [11] W. P. Dong, P. J. Sullivan, K. J. Stout, Comprehensive study of parameters for characterizing three dimensional surface topography II: Statistical properties of parameter variation. *Wear* 167 1993 9-21.
- [12] Czanderna, T. V. Vorburger, Plenum Press, *Beam Effects, Surface Topography, and depth Profiling in Surface Analysis*, 1998.
- [13] R. Ohlsson, A. Wihlborg, H. Westberg, The accuracy of fast 3D topography measurements, *International Journal Of Machine Tools and Manufacture*, 41 2001 1899-1907.
- [14] W. P. Dong, P. J. Sullivan, K. J. Stout, Comprehensive study of parameters for characterizing three dimensional surface topography IV: Parameter for characterising spatial and hybrid properties. *Wear* 178 1994 45-60.
- [15] S. Ganti, B. bhushan, Generalized fractal analysis and its applications to engineering surfaces, *Wear*, 180 1995 17-34.
- [16] T. R. Thomas, B. -G. Rosen, N. Amini, Fractal Characterisation of the anisotropy of rough surfaces, *Wear*, 232 1999 41-50.
- [17] C. Roques-Carnes, N. Bodin, G. Monteil, J. F. Quiniou, Description of rough surface using conformal equivalent structure concept. Part 1. Stereological Approach, *Wear*, 248 2001 82-91.
- [18] C. Roques-Carnes, N. Bodin, G. Monteil, J. F. Quiniou, Description of rough surface using conformal equivalent structure concept. Part 2. Numerical approach, *Wear*, 248 2001 92-99.
- [19] P. G. Benardos, G. -C. Vosniakos, Predicting surface roughness in machining: a review, *International Journal of Machine Tools and Manufacture*, 43 2003 833-844.
- [20] A. M. Ramos, C. Relvas, A. Simões, The influence of finishing milling strategies on texture roughness and dimensional deviations on the machining of complex surface, *Journal of Materials Processing Technology* 136 (2003) 209-216.
- [21] R. Baptista, J. F. Antune Simoes, Three and five axes milling of sculptured surfaces, *Journal of Materials Processing Technology*, 103 2000 398-403.
- [22] D.A. Axinte, R. C. Dewes, Surface integrity of hot work tool steel after high speed milling-experimental data and empirical models, *Journal of Materials Processing Technology*, 127 2002 325-335.
- [23] Y. -H. Jung, J. -S. Kim, S. -M. Hwang, Chip load prediction in ball-end milling, *Journal of Materials Processing Technology*, 111 2001 250-255.
- [24] J. Y. Jung, C. M. Kim, T. J. Ko, W. J. Chung, optimization for improvement of surface roughness in high speed machining, *Current Advances in Mechanical Design and Production*, 8 2004 953-960.
- [25] B. H. Kim, C. N. Chu, Texture prediction of milled surfaces using texture superposition method, *Computer Aided Design*, 31 1999 485-494.
- [26] K. -D. Bouzakis, P. Aichouh, K. Efstahiou, Determination of the chip geometry, cutting force and roughness in free form surfaces finishing milling, with ball end tools, *International Journal of Machine Tools & Manufacture*, 43 2003 499-514.
- [27] C.K. Toh. Surface topography analysis in high speed finish milling inclined hardened steel, *Precision Engineering*, 28 2004 386-398.